University of Groningen

Andromeda XXV - A dwarf galaxy with a low central dark matter density

Charles, Emily J.E.; Collins, Michelle L.M.; Michael Rich, R.; Read, Justin I.; Kim, Stacy Y.; Ibata, Rodrigo A.; Martin, Nicolas F.; Chapman, Scott C.; Balbinot, Eduardo; Weisz, Daniel R.

IMPORTANT NOTE: You are advised to consult the publisher's version (publisher's PDF) if you wish to cite from it. Please check the document version below.

Document Version
Publisher's PDF, also known as Version of record

Publication date:
2023

Link to publication in University of Groningen/UMCG research database

Andromeda XXV – a dwarf galaxy with a low central dark matter density

Emily J. E. Charles [1]★ Michelle L. M. Collins [1], R. Michael Rich [2], Justin I. Read [1], Stacy Y. Kim,[1] Rodrigo A. Ibata,[3] Nicolas F. Martin [3], Scott C. Chapman,[4] Eduardo Balbinot [5] and Daniel R. Weisz [6]

[1]*Physics Department, University of Surrey, Guildford GU2 7XH, UK*
[2]*Department of Physics and Astronomy, University of California at Los Angeles, Los Angeles, CA 90095, USA*
[3]*Observatoire astronomique de Strasbourg, Universié de Strasbourg, CNRS, UMR 7550, 11 rue de l'Université, Strasbourg F-67000 , France*
[4]*Department of Physics and Atmospheric Science, Dalhousie University, Coburg Road, Halifax B3H1A6, Canada*
[5]*Kapteyn Astronomical Institute, University of Groningen, Landleven 12, AD Groningen NL-9747, the Netherlands*
[6]*Department of Astronomy, University of California Berkeley, Berkeley, CA 94720, USA*

ABSTRACT

Andromeda (And) XXV has previously been reported as a dwarf spheroidal galaxy (dSph) with little-to-no dark matter. However, the uncertainties on this result were significant. In this study, we nearly double the number of member stars and re-derive the kinematics and mass of And XXV. We find that And XXV has a systemic velocity of $v_r = -107.7 \pm 1.0$ kms^{-1} and a velocity dispersion of $\sigma_v = 3.7^{+1.2}_{-1.1}$ kms^{-1}. With this updated velocity dispersion and a new literature measurement of the radial surface brightness profile, we derive a mass contained within the half-light radius of $M(r < r_h) = 4.7^{+3.0}_{-2.9} \times 10^6$ M$_\odot$. This mass corresponds to a mass-to-light ratio of $[M/L]_{r_h} = 25^{+17}_{-16}$ M$_\odot$/L$_\odot$, demonstrating that And XXV is most-likely dark matter dominated. We also measure the metallicity of And XXV to be [Fe/H] $= -1.9 \pm 0.1$ dex, which is in agreement with previous results. Finally, we extend the analysis of And XXV to include mass modelling using `GravSphere`. We find that And XXV has a low central dark matter density, $\rho_{DM}(150\,\text{pc}) = 2.3^{+1.4}_{-1.1} \times 10^7$ M$_\odot$ kpc^{-3}, which makes And XXV a clear outlier when compared to other local group dSphs of the similar stellar mass. In a companion paper, we will explore whether some combination of dark matter cusp-core transformations and/or tides can explain And XXV's low density.

Key words: galaxies: dwarf – galaxies: kinematics and dynamics – galaxies: haloes – dark matter.

1 INTRODUCTION

Dwarf galaxies are typically dark matter dominated systems, with mass-to-light ratios in the range 10–1000s, making them ideal systems for testing dark matter physics and cosmology (e.g. Mateo 1998; Tolstoy, Hill & Tosi 2009; Simon 2019). The most successful cosmological model to date is Lambda Cold Dark Matter (ΛCDM), which explains the cosmic microwave background radiation (e.g. Peebles 1982; Komatsu et al. 2009; Aubourg et al. 2015; Planck Collaboration et al. 2016, 2020), nucleosynthesis (e.g. Walker et al. 1991; Smith, Kawano & Malaney 1993; Burles et al. 1999; Cyburt 2004; Steigman 2007; Fields 2011), and structure formation on large scales (e.g. Bond, Kofman & Pogosyan 1996; Springel et al. 2005; Gao, Springel & White 2005a; Gao et al. 2005b; Tegmark et al. 2006; Springel, Frenk & White 2006), albeit by invoking three mysterious components – dark matter, dark energy, and inflation (Planck Collaboration et al. 2016, 2020). However, on galactic scales, particularly dwarf galaxies, there have been a number of long-standing tensions between ΛCDM predictions and observations (e.g. Bullock & Boylan-Kolchin 2017; Buckley & Peter 2018; Sales, Wetzel & Fattahi 2022). One such tension is the so-called 'cusp-core' problem (Moore 1994; Flores & Primack 1994; de Blok 2010; Navarro et al. 2010; Walker & Peñarrubia 2011; Read et al. 2017;

Genina et al. 2018; Read, Walker & Steger 2019), which arises when comparing the dark matter density profiles of dwarf galaxies from dark matter only simulations in a ΛCDM cosmology to observations of dwarf galaxies. ΛCDM predicts that the dark matter inside dwarf galaxies should follow a universal 'cusped' profile that has a highly dense centre that steeply decreases with radius, such that $\rho_{DM} \propto r^{-1}$ (Dubinski & Carlberg 1991; Navarro, Frenk & White 1996b, 1997; Moore et al. 1999). Instead, a growing number of dwarfs have been observed with 'cored' dark matter profiles described by a shallow central density that remains roughly constant in the centre, such that $\rho_{DM} \sim$ constant (Flores & Primack 1994; Moore 1994; de Blok et al. 2001a, b; de Blok 2010; Marchesini et al. 2002; Simon et al. 2005; Battaglia et al. 2008; Walker et al. 2010; Agnello & Evans 2012; Amorisco & Evans 2012; Newman et al. 2013; Read et al. 2017; Read et al. 2019).

For many of the cored dwarfs observed, a plausible solution to the cusp-core problem within the ΛCDM paradigm is dark matter heating. This is the process of sudden gas removal due to stellar winds, dynamical friction or supernovae feedback which results in gravitational fluctuations, causing the dark matter halo to expand. When this process is repeated across many cycles of star formation the dark matter halo expands irreversibly, reducing the central dark matter density and flattening the cusped profile into a core over time (Navarro, Eke & Frenk 1996a; Gnedin & Zhao 2002; Read & Gilmore 2005; Mashchenko, Wadsley & Couchman 2008; Pontzen & Governato 2012; Zolotov et al. 2012; Brooks & Zolotov 2014;

★ E-mail: e.charles@surrey.ac.uk

Oñorbe et al. 2015; Tollet et al. 2016; Read, Agertz & Collins 2016; Read et al. 2019). However, dark matter heating is only proposed to be effective in galaxies with extended star formation (Read et al. 2016; Read et al. 2019) that are above a stellar-mass-to-halo-mass ratio threshold of $M_*/M_{200} \sim 5 \times 10^{-4}$ (Di Cintio et al. 2014, but see Orkney et al. (2021)).

Puzzlingly, there is a subset of dwarfs within the low surface brightness population of the Local Group (LG) with M_*/M_{200} below this threshold with unusually low central densities that are unlikely to be explained by dark matter heating alone. Around the Milky Way (MW) two such dwarfs have been found, Crater II (Torrealba et al. 2016) and Antlia II (Torrealba et al. 2019). Similarly around Andromeda (M31) two more have been observed, Andromeda XIX (McConnachie et al. 2008; Collins et al. 2020) and Andromeda XXI (Martin et al. 2009; Collins et al. 2021). These systems have a diffuse nature, described by a large half-light radius and very low surface brightness. Furthermore, the mass contained within the half-light radius for these systems, determined from velocity dispersions measurements, is less massive than other galaxies with similar size and brightness (Caldwell et al. 2017; Fu, Simon & Alarcón Jara 2019; Torrealba et al. 2019; Collins et al. 2020, 2021), meaning that it is likely that these systems reside in low mass and low density dark matter halos. While detailed star formation histories for these systems are not currently available to completely rule out dark matter heating as the cause, even under the (unlikely) assumption of highly efficient dark matter heating, their low densities cannot be reproduced (Torrealba et al. 2019; Collins et al. 2021). Instead, tidal interactions with the host (MW or M31) are the suspected culprit causing the low density dark matter halos of these systems (Torrealba et al. 2019; Fu et al. 2019; Collins et al. 2021).

In this paper, we investigate another potential outlier, Andromeda XXV (And XXV), a dSph satellite galaxy of M31 first discovered as part of the Pan-Andromeda Archaeological Survey (Richardson et al. 2011). And XXV was previously identified as a potential outlier within the LG in a 2013 study (Collins et al. (2013), hereafter known as C13) that performed a kinematic analysis of numerous M31 dSph satellites. And XXV was found to have a low velocity dispersion, $\sigma_v = 3.0^{+1.2}_{-1.0}$ kms^{-1}, which results in a mass-to-light ratio of $[M/L]_{r_h} = 10.3^{+7.0}_{-6.7}$ M$_\odot$/L$_\odot$. This is consistent with a dark matter dominated system. However, due to the small number of member stars (26) with stellar kinematics in their sample, the uncertainty on this value is significant. As such, within the uncertainties the presence of dark matter is not required and And XXV could be described by a simple stellar system with no appreciable dark matter component. C13 point out, more stellar velocities are needed to confirm or rule out the presence of dark matter in this system. We present a revised kinematic analysis, using the spectroscopic data set outlined in C13 combined with new observations to provide a larger sample size, nearly double that used in C13, allowing us to critically reassess if And XXV really is a dSph with no appreciable dark matter. We will also extend the analysis to investigate the metallicity of And XXV. Finally we use the dynamical mass modelling tool `BINULATOR + GravSphere` (Read & Steger 2017; Read, Walker & Steger 2018; Read et al. 2019; Gregory et al. 2019; Genina et al. 2020b; Collins et al. 2021; Read et al. 2021), to gain an insight into the dark matter content of And XXV.

The outline of the paper is as follows: in Section 2 we detail the photometric and spectroscopic observations used in this study. We detail the contaminant removal procedure used to remove MW and M31 contaminant stars from our sample in Section 3 and discuss our kinematic analysis of And XXV in Section 4. In Section 5 we investigate the metallicity of And XXV. Next, we outline the dynamical mass modelling results for And XXV Section 6. In Section 7 we discuss our results and finally we conclude in Section 8.

2 OBSERVATIONS

2.1 Deep extragalactic imaging multi-object spectrograph spectroscopy

The spectroscopic data for And XXV were obtained using the Deep Extragalactic Imaging Multi-Object Spectrograph (DEIMOS) Faber et al. (2003), Cooper et al. (2012) mounted on the Keck II telescope. The observations are comprised of two masks. The first was taken in September 2010 (previously presented in C13), and the second mask was observed on 2018 August 18. The instrumental setup was the same for both masks, using a 1200 line mm^{-1} grating with a resolution of 1.3 Å. To determine the velocity and metallicity of each member star, we use the calcium triplet (Ca(II)) lines. The Ca(II) lines are present in the region around ~ 8500 Å. As such our observations targeted the wavelength range of ~ 5600–9800 Å with a central wavelength of 7800 Å to resolve the Ca(II) lines. Each mask was split into 3×20 min exposures, combining to give a total exposure time of 3600 s per mask. The average seeing was ~ 0.8 arcsec for both masks, which resulted in an average signal-to-noise ratio (S/N) of ~ 5 per pixel ($M_V < 21$: S/N~ 16, $21 \leq M_V < 24$: S/N~ 6, $M_V > 24$: S/N~ 2).

The data were reduced using a custom pipeline, described in detail in Ibata et al. (2011) and C13. In short, the pipeline detects and removes cosmic rays, then corrects for scattered light, slit function, illumination, and fringing. To account for pixel-to-pixel variations flat-fielding was performed. Next wavelength calibrations of each pixel were conducted using arc-lamp exposures. Then, the sky was subtracted from the two-dimensional spectra. Finally, each spectrum was extracted (without resampling) from a small spatial region around each target. The velocities and corresponding uncertainties for all stars were derived using the strong Ca(II) triplet feature found in the spectra of the non-resampled data. A Markov Chain Monte Carlo (MCMC) routine fit a Gaussian to the three Ca(II) triplet lines and determined the offset of the line compared to the known rest-frame wavelengths. This shift was converted into a velocity. The final value for the velocity uncertainty comprises of the uncertainty from the MCMC posterior distribution combined with the uncertainty inherent to DEIMOS and the reduction pipeline which was taken to be 3.2 kms^{-1} (Collins et al. 2020). This is similar to the uncertainty of 3.4 kms^{-1} found in Martin et al. (2014) for the same type of targets. The results from each mask were combined into a single catalogue.

Misalignments of the slitmasks can cause velocity shifts of up to 15 kms^{-1}. We correct for these by comparing atmospheric models to the telluric absorption lines in the spectrum to shift the spectra to the correct frame as described in C13. To further confirm if any significant misalignment had occurred we check for a velocity error gradient across the mask. None were found in either mask. Finally, there were a few stars present both masks which were compared to ensure the velocity uncertainties were well measured.

2.2 Large binocular telescopelarge binocular cameras photometry

The photometric data for And XXV were obtained using the Large Binocular Cameras (LBC) mounted on the Large Binocular Telescope (LBT) in the V_{Bessell}- and i_{SLOAN}-band. Observations were

conducted on the nights of 2011 October 28 and November 8 with a seeing that was ranging from 0.7 arcsec to 1.2 arcsec. With its 4i say Charge-Coupled Devices (CCDs), the cameras both cover an area of about 23×25 arcmin^2. In total, 29 exposures of 360 s were taken with each filter, for a total exposure time of 2.9 h per band.

The raw photometry was reduced using the Cambridge Astronomical Survey Unit (CASU) pipeline where the images are debiased, flat-fielded, trimmed, and gain-corrected (Irwin & Lewis 2001). The reduced photometric data were made into a catalogue. Each datum was then morphologically categorized to distinguish between stellar, non-stellar (e.g. background galaxies) or noise-like objects. Only stellar objects were considered for further analysis. Finally, the data were extinction corrected using the dust maps from Schlafly & Finkbeiner (2011), using $A_V = 0.270$ mag and $A_i = 0.171$ mag.

The photometric and spectroscopic observations were combined by cross-matching the on-sky position of each star within an allowed tolerance of ± 1 arcsecond.

3 SELECTING MEMBERS OF ANDROMEDA XXV

Before we can perform the kinematic analysis of And XXV we must identify the most probable members of And XXV and remove any contaminants from the MW or M31 halo. It is difficult to differentiate between member and contaminant stars using velocity information alone. This is especially true for foreground MW stars as the two systems have similar systemic velocities. Instead, to determine likely member stars, we use a 'triple-threat' probabilistic approach which was first outlined in Tollerud et al. (2012) and C13, then further developed in Collins et al. (2020), Collins et al. (2021) and Gregory et al. (2019). The method assigns each star a probability of membership using three probability criteria: (1) the star's position on the sky with relation to the centre of And XXV, P_{dist}; (2) the star's position on a colour magnitude diagram (CMD) of And XXV, P_{CMD}; and (3) the velocity of the star, P_{vel}. We discuss each of these criteria in more detail below.

3.1 Distance probability

P_{dist} is determined using radial surface brightness profile modelled as:

$$P_{\text{dist}} = \exp\left[-\left(\frac{r^2}{2\eta_{\text{dist}} r_p^2}\right)\right] \tag{1}$$

where r is the radial distance of the star from the centre of And XXV (taken to be $0^h30^m9.9^s$ - RA, $46^{circ}51'41''$ - Dec Martin et al. (2016)) and η_{dist} is a free parameter used to scale the exponential profile to the size of And XXV. η_{dist} was extensively tested for any potential biases or dependencies and a final value of $\eta_{\text{dist}} = 2.5$ was used. r_p used to modify the half-light radius, r_h, to account for any ellipticity, described by:

$$r_p = \frac{r_h(1 - \epsilon)}{1 + \epsilon \cos(\theta)} \tag{2}$$

where $r_h = 2.7$ arcmin (Martin et al. 2016; Savino et al. 2022), ϵ is the ellipticity ($\epsilon = 0.03$) and θ is the stars angular position with respect to the dwarfs major axis ($\theta = -16\,^\circ$) (Martin et al. 2016).

3.2 Colour-magnitude diagram probability

P_{CMD} is determined using the colour-magnitude diagram of And XXV. A by-eye best-fit isochrone was overlaid onto the CMD

to identify the stars most likely to be red giant branch stars of And XXV. The isochrone used was an old, metal-poor isochrone ([Fe/H] $= -1.9$ dex, [α/Fe] $= 0.0$ dex, age $= 12$ Gyr) obtained from the DARTMOUTH stellar evolutionary models Dotter et al. (2008) shifted to the distance modulus of And XXV, $m - M = 24.38$ (Savino et al. 2022)). The CMD of And XXV and the by-eye best-fit isochrone are shown in the right panel of Fig. 1. The minimum distance in colour-magnitude space, d_{min}, of each star to the isochrone was converted into a probability of membership using:

$$P_{\text{CMD}} = \exp\left[-\left(\frac{d_{\text{min}}^2}{2\eta_{\text{CMD}}^2}\right)\right] \tag{3}$$

where η_{CMD} is another free parameter, this time used to account for the scatter of stars around the best-fit isochrone. Again, this free parameter was tested for any potential biases or dependencies and a final value of $\eta_{\text{CMD}} = 0.2$ was chosen.

3.3 Velocity probability

P_{vel} is determined by simultaneously fitting the velocities for all of the stars in the spectroscopic observations by assuming that these stars inhabit a profile of four dynamically distinct peaks. Four Gaussians are used to describe the different peaks which correspond to And XXV stars ($P_{\text{And XXV}}$), then M31 halo contaminant stars (P_{M31}) and two peaks for the MW contaminant stars (P_{MW1}, P_{MW2}). The MW velocity profile is often assumed to be a single distribution for contaminant removal purposes. However, due to the similarity in systemic velocity for And XXV and the MW, for our study, this assumption is not valid. Instead, we need to include this complexity in our model by modelling the MW as two velocity distributions (e.g. Gilbert et al. 2006). Each Gaussian is defined by a systemic velocity (v_r) and a velocity dispersion (σ_v), such that the probability of each star belonging to each peak ($P_{\text{And XXV}}$, P_{M31}, P_{MW1} and P_{MW2}) is:

$$P_{\text{peak}} = \frac{1}{\sqrt{2\pi}\sqrt{\sigma_{v_{\text{peak}}}^2 + v_{\text{err,i}}^2}} \times \exp\left(-\frac{1}{2}\left[\frac{v_{\text{peak}} - v_i}{\sqrt{\sigma_{v_{\text{peak}}}^2 + v_{\text{err,i}}^2}}\right]^2\right) \tag{4}$$

where v_i and $v_{\text{err,i}}$ are the velocity and velocity uncertainty of a given star respectively. The overall log-likelihood function is therefore described by:

$$\log(\mathcal{L}) = \sum_{i=1}^{N}(\alpha P_{\text{And XXV}} + \beta P_{\text{M31}} + \gamma P_{\text{MW1}} + \delta P_{\text{MW2}}) \tag{5}$$

where α, β, γ, and δ are constants describing the proportion of stars belonging to And XXV, M31, MW1, and MW2, respectively, and are normalized, such that $\alpha + \beta + \gamma + \delta = 1$. The components of this likelihood function were found using emcee, a python MCMC package (Foreman-Mackey et al. 2013). The routine used 200 walkers, over 5000 iterations with a burn-in stage of 1550 and uniform flat priors were introduced for each parameter, see Table. 1 for a summary of the priors and results for the MCMC analysis.

It is important to note that, while the velocity and velocity dispersion values will likely resemble the final values, this is not the final kinematic result for And XXV. It is only used to determine P_{vel}. This is because it does not consider the impact of any potential M31 or MW contamination in the wings of the And XXV Gaussian, hence why the other two probability filters are important and the combination of all three filters is used to weight the likelihood function in the final kinematic analysis. The probability distribution described by the Gaussian for each peak can then be combined to
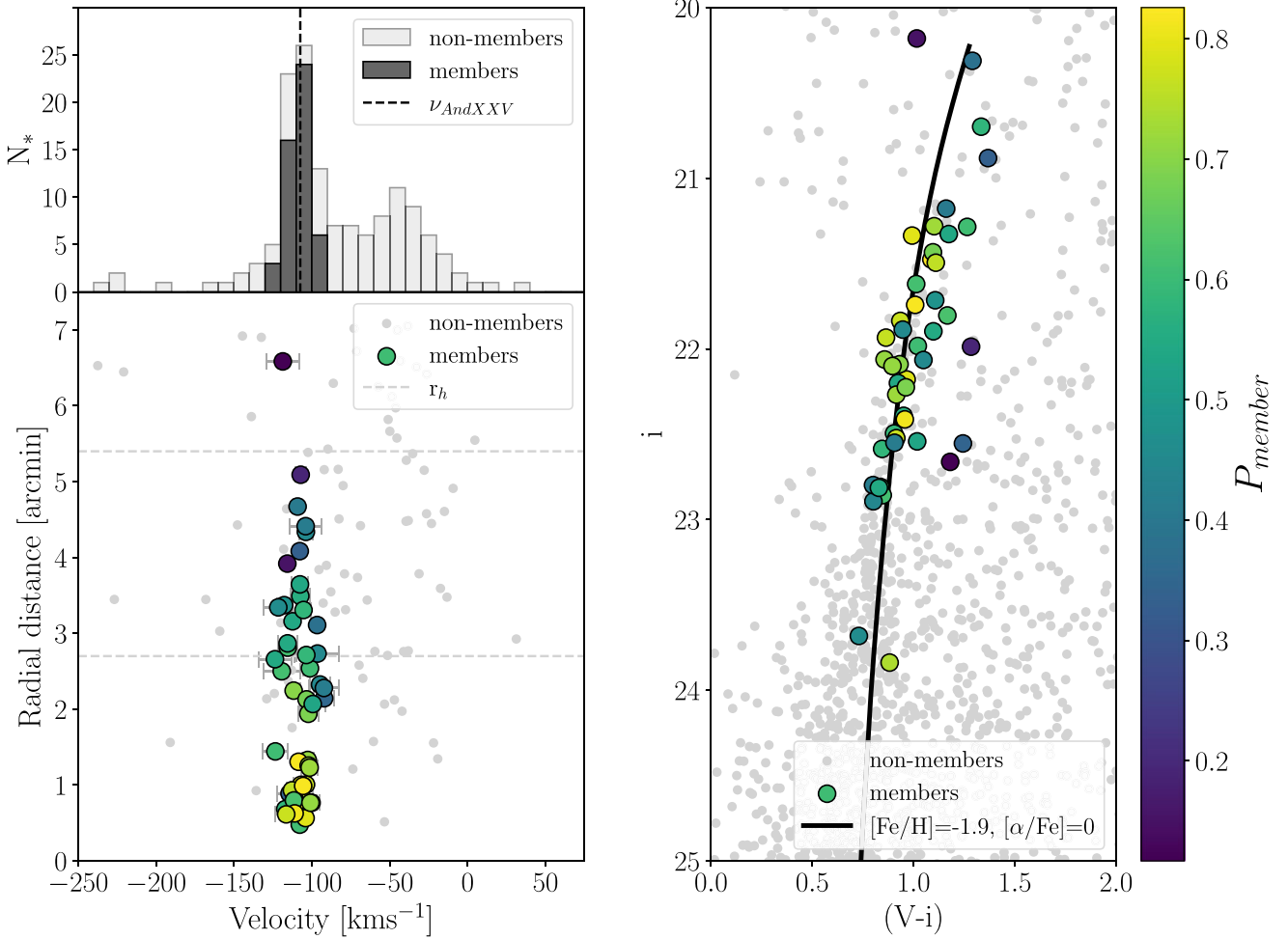
Figure 1. *Left top:* The velocity histogram from And XXV. Light grey represents non-members likely contamination from foreground MW stars or M31 halo stars. Dark grey represents the 49 identified member stars of And XXV. The black dashed line represents the systemic velocity of And XXV determined in this study. *Left bottom:* Radial distance from the centre of And XXV as a function of the line of sight velocity. The smaller light grey circles are the non-member stars from the spectroscopic data. The larger coloured circles are the member stars, colour-coded by the probability of membership (see colour bar on the right) and the error bars are the 1σ uncertainties. The horizontal grey dashed lines represent $1\times$ and $2\times$ r_h from the bottom up respectively. *Right:* The colour magnitude diagram for And XXV. Again the smaller light grey circles are non-member stars within $1.5\times$ r_h and the larger coloured circles are the member stars colour-coded by the probability of membership. The black solid line is a by-eye best-fit isochrone ([Fe/H] $= -1.9$ dex, [α/Fe] $= 0.0$ dex, age $= 12$ Gyr) for And XXV taken from the DARTMOUTH stellar evolutionary models Dotter et al. (2008) and shifted to the distance modulus of And XXV, $m - M = 24.38$ (Savino et al. 2022)).

Table 1. Prior values and results for the variables used in our emcee analysis for $P_{\rm vel}$. [*] *Note:* This is not the final systemic velocity and velocity dispersion value for And XXV - it is only used to determine $P_{\rm vel}$.

Priors:		
Peak	$\nu_{\rm r}$ (kms^{-1})	σ_ν (kms^{-1})
$P_{\rm And\ XXV}$	$-130 < \nu_{\rm r} < -90$	$0 < \sigma_\nu < 50$
$P_{\rm M31}$	$-400 < \nu_{\rm r} < -130$	$0 < \sigma_\nu < 200$
$P_{\rm MW1}$	$-60 < \nu_{\rm r} < 50$	$0 < \sigma_\nu < 100$
$P_{\rm MW2}$	$-90 < \nu_{\rm r} < -50$	$0 < \sigma_\nu < 100$
Results:		
Peak	$\nu_{\rm r}$ (kms^{-1})	σ_ν (kms^{-1})
$P_{\rm And\ XXV}$	$-107.6^{+1.5}_{-1.4}$	$5.1^{+2.3}_{-2.0}$ [*]
$P_{\rm M31}$	$-272.2^{+50.8}_{-46.6}$	$132.1^{+30.7}_{-28.0}$
$P_{\rm MW1}$	$-45.3^{+14.5}_{-9.2}$	$27.2^{+10.7}_{-9.3}$
$P_{\rm MW2}$	$-71.1^{+7.8}_{-11.4}$	$38.6^{+15.5}_{-7.9}$

give $P_{\rm vel}$, using:

$$P_{\rm vel} = \frac{P_{\rm AndXXV}}{P_{\rm MW1} + P_{\rm MW2} + P_{\rm M31} + P_{\rm AndXXV}} \quad (6)$$

The final probability of membership to And XXV for each star is the product of the three probability cuts, such that:

$$P_{\rm member} = P_{\rm dist} \times P_{\rm CMD} \times P_{\rm vel} \quad (7)$$

Stars with a probability of $P_{\rm member} > 0.10$ were considered member stars. The probability of membership cut-off is kept intentionally low as we use the velocity dispersion for the kinematic analysis. Hence, we do not want to artificially decrease the velocity dispersion by removing potential candidates with a probability cut that is too strict. Furthermore, all non-members have a probability of membership significantly below this cut-off point. A total of 49 members were identified (as shown in Fig. 1). These data contain nearly double the number of members compared to that used in C13.
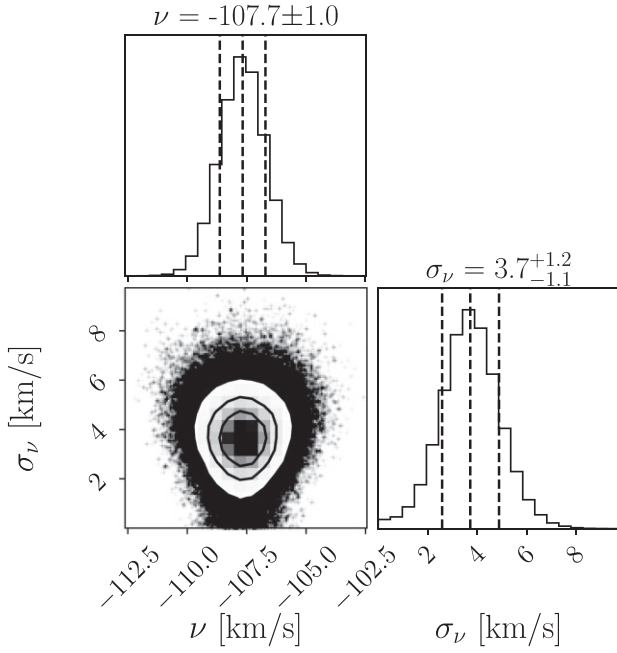
Figure 2. A corner plot showing the results of our kinematic analysis using EMCEE. The velocity and velocity dispersion are well resolved, giving $\nu_r = -107.7 \pm 1.0$ km s^{-1} and $\sigma_\nu = 3.7^{+1.2}_{-1.1}$ kms^{-1}.

4 KINEMATIC ANALYSIS OF ANDROMEDA XXV

We used another `emcee` routine to determine the velocity (ν) and velocity dispersion (σ_ν) of And XXV. This time, the routine fits a single Gaussian for the 49 member stars, with the likelihood of each star weighted by the star's respective probability, such that the log-likelihood function is:

$$\log(\mathcal{L}) = \sum_{i=1}^{N} \log(P_{\text{member}_i} P_{\text{AndXXV}_i}) \qquad (8)$$

The routine used 500 walkers over 5000 iterations with a burn-in stage of 3750. The values of ν and σ_ν for And XXV from the P_{vel} analysis were used as initial guesses and the same flat priors used for P_{vel} were implemented. The resulting posterior distribution can be seen in Fig. 2.

4.1 Kinematic results

The velocity and velocity dispersion are well resolved, giving $\nu = -107.7 \pm 1.0$ km s^{-1} and $\sigma_\nu = 3.7^{+1.2}_{-1.1}$ km s^{-1}, the uncertainties are the 1σ uncertainty intervals from the posterior distributions. The properties derived for And XXV are listed in Table 2. The velocity and velocity dispersion are consistent with those derived in C13 ($\nu = -107.8 \pm 1.0$ km s^{-1}, $\sigma_\nu = 3.0^{+1.2}_{-1.0}$ km s^{-1}) although our velocity dispersion is slightly higher. This is likely due to the targeting of the C13 study. The first mask preferentially targeted stars close to the centre of And XXV. As seen in Fig. 1, the central stars are kinematically colder than those in the outskirts (velocity dispersion of ~ 2.3 km s^{-1} in the centre versus ~ 5.7 km s^{-1} on the outskirts). The outermost stars included in the new spectroscopic data set increase the average dispersion measured in this study. It is important to note that at the outskirts of And XXV we are more susceptible to contamination from non-member stars, especially due

Table 2. The properties of And XXV. Sources a: Martin et al. (2016), b: Savino et al. (2022), c: this work.

Property	Value	Source
α, δ (J2000)	$00:30:09.9 + 46:51:41$	a
m_V	$15.3^{+0.3}_{-0.2}$	a
M_V	$-9.1^{+0.3}_{-0.2}$	b
D (kpc)	751.6^{+25}_{-21}	b
r_h (arcmin)	$2.7^{+0.4}_{-0.3}$	a, b
r_h (pc)	590^{+90}_{-47}	a, b
L (L$_\odot$)	$3.7^{+0.4}_{-0.5} \times 10^5$	b
ν (kms^{-1})	-107.7 ± 1.0	c
σ_ν (kms^{-1})	$3.7^{+0.4}_{-0.5}$	c
M(r< r$_h$) (M$_\odot$)	$4.7^{+3.0}_{-2.9} \times 10^6$	c
[M/L]$_{r_h}$ (M$_\odot$/L$_\odot$)	25^{+17}_{-16}	c
[Fe/H] (dex)	-1.9 ± 0.1	c
ρ_{DM}(150 pc) (M$_\odot$ kpc^{-3})	$2.3^{+1.4}_{-1.1} \times 10^7$	c

to the similarity in velocity between And XXV and the foreground MW stars. We extensively tested our membership selection; however, it is possible inclusion of contaminates could potentially contribute to the velocity flaring at larger radii. Furthermore, due to the size of the uncertainties on the two bins, likely arising from small number statistics, the velocity flaring observed is statistically insignificant within 1σ.

Using the now better constrained velocity dispersion, we can measure the mass, $M(r < r_h)$, and mass-to-light ratio, $[M/L]_{r_h}$, contained within the half-light radius of And XXV. Assuming a flat velocity dispersion profile, $M(r < r_h)$ can be calculated using Walker et al. (2009):

$$M(r < r_h) = 580 \, r_h \, \sigma_\nu^2 \qquad (9)$$

The mass of And XXV was determined to be $M(r < r_h) = 4.7^{+3.0}_{-2.9} \times 10^6$ M$_\odot$, which is in agreement with the C13 study within the 1σ uncertainties. Using the updated absolute magnitude value of And XXV, $M_V = -9.1$ (Savino et al. 2022), which is equal to a luminosity of $L = 3.7^{+1.4}_{-0.5} \times 10^5$ L$_\odot$, the mass-to-light ratio contained within the half-light radius is $[M/L]_{r_h} = 25^{+17}_{-16}$ M$_\odot$/L$_\odot$. The mass-to-light ratio agrees with the value from C13 within the 1σ uncertainties and demonstrates that And XXV is dark matter dominated. Although, assuming Gaussian uncertainties, And XXV is still consistent with a simple stellar system of $[M/L]_{r_h} < 5$ with $\sim 1.25\sigma$. Furthermore, if we instead use the previous luminosity value ($L = 6.8 \times 10^5$ L$_\odot$) with the updated velocity dispersion we derive a mass-to-light ratio of $[M/L]_{r_h} = 15^{+10}_{-9}$ M$_\odot$/L$_\odot$ This demonstrates that the increase in the mass-to-light ratio is due to the combination of the slightly increased velocity dispersion and the updated luminosity value that is almost half the previous value that was used in C13.

4.2 Comparison to kinematics of local group dSphs

Dwarf galaxies are typically dark matter dominated systems at all radii and as such we would expect them to have mass-to-light ratios of $[M/L]_{r_h} > 10$ M$_\odot$/L$_\odot$. The left panel of Fig. 3 shows the mass-to-light ratios of LG dSphs, the light grey circles and triangles are M31 and MW dSphs, respectively, taken from Tollerud et al. (2012); Collins et al. (2013); Collins et al. (2017); Collins et al. (2020); Collins et al. (2021); Walker et al. (2007); Walker et al. (2009); Simon & Geha (2007); Simon et al. (2011); Simon et al. (2015);
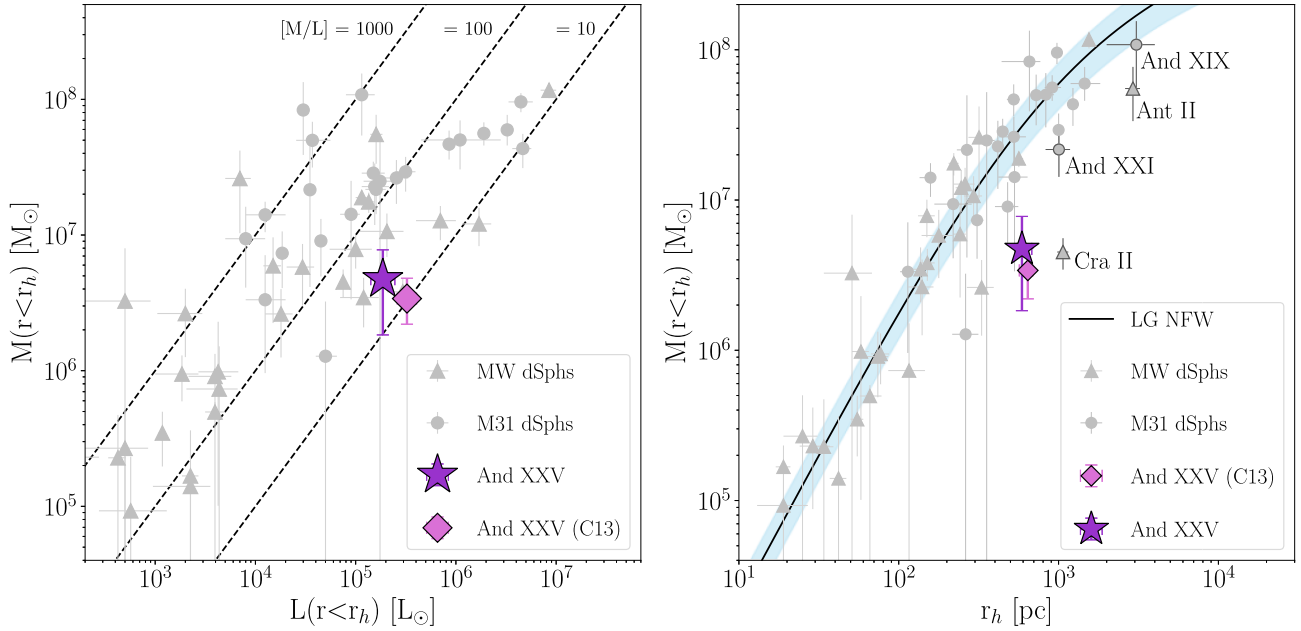
Figure 3. Left: Mass-to-light ratios of dSphs in the LG. The diagonal black lines illustrate a mass-to-light ratio of 10, 100 and 1000 from right to left respectively. Right: The mass contained within the half-light radius for the LG dSphs. The solid black line is the best-fitting NFW mass profile for the LG population (Collins et al. 2014), with the 1σ uncertainties for this relationship shown by the blue shaded region. Both: The light grey triangles are MW dSphs and the light grey circles are M31 dSphs. The C13 result is illustrated by the pink diamond and the updated value from this study for And XXV is shown by the purple star. For all data points, the error bars show the 1σ uncertainties.

Martin et al. (2007); Martin et al. (2013a); Martin et al. (2013b); Martin et al. (2014); Ho et al. (2012); Kirby, Simon & Cohen (2015); Kirby et al. (2017). The pink diamond shows the C13 result. This mass-to-light ratio was indicative of a dark matter dominated system, but within the uncertainties did not require the presence of dark matter. The purple star shows the mass-to-light ratio of And XXV derived from this study. We can see that with the combination of the slightly increased velocity dispersion and updated luminosity used in this study, the mass-to-light ratio of And XXV is that of a dark matter dominate system and moves in line with other LG dSphs.

The right panel of Fig. 3 shows the mass contained within the half-light radius as a function of the half-light radius for the LG dSphs. Again the light grey circles and triangles are M31 and MW dSphs, respectively, taken from the same sources. With the updated velocity dispersion the half-light radius mass moves more in line with what we would expect (compare the pink diamond – C13 to the purple star – this study). Despite this, we can see that the mass of And XXV is still significantly lower when compared to the best-fitting NFW mass profile for the LG population (Collins et al. 2014), illustrated by the solid black line and the light blue shaded region is the 1σ uncertainty. This extended radial behaviour with significantly less mass than expected for its size is also shown by the other four outliers And XXI (Collins et al. 2021), And XIX (Collins et al. 2020), Crater II (Torrealba et al. 2016), and Antlia II (Torrealba et al. 2019), as highlighted in Fig. 3. For these systems, it is suspected that tides have caused the low masses. Furthermore, C13 noted that tidal interactions could have acted to lower the central density of And XXV, and the increase in velocity dispersion with radius could indicate a tidal influence.

To investigate if we can observe the impact of tides in the kinematics, we altered the Gaussian component of the likelihood function described in equation (4) to include a velocity gradient component that would indicate the presence of tidal streams, following the methodology outlined in Martin & Jin (2010). No statistically significant velocity gradient was found. It is important to note that this does not mean And XXV has not experienced tidal influences, especially as we potentially run into the same small number statistics issues reported by the C13 as we are trying to fit more parameters than the simple Gaussian outlined in equation (4). We return to the potential impact of tides on And XXV in Section 7.

5 METALLICITY OF ANDROMEDA XXV

We determined the metallicity of And XXV by measuring the equivalent widths of the Ca(II) triplet lines from the spectroscopic observations. These absorption lines are a good proxy for iron abundance [Fe/H] (Armandroff & Da Costa 1991). We focused on the equivalent widths of the Ca(II) triplet feature in the co-added spectra for And XXV. We only include member stars with a good signal-to-noise ratio (S/N), for our data set, this was determined to be $S/N > 2.5$ per pixel, which resulted in a sample that comprised of 32 stars. To calculate the equivalent widths, we followed the methodology outlined in C13. Firstly, we apply a Doppler correction to each star to ensure the spectra are measured in the rest frame. The spectra were then interpolated onto a common framework before co-adding the S/N weighted spectra. Next, the spectra were normalized, such that the mean continuum was equal to one. Finally, we simultaneously fit the continuum and three Gaussian peaks to each of the three Ca(II) triplet lines to obtain the equivalent widths, see Fig. (4).

The metallicity was determined from the equivalent widths using the approach described by Starkenburg et al. (2010) such that:

$$[\text{Fe/H}] = -2.87 + 0.195\,M + 0.48\,\Sigma Ca - 0.913\,\Sigma Ca^{-1.5}$$
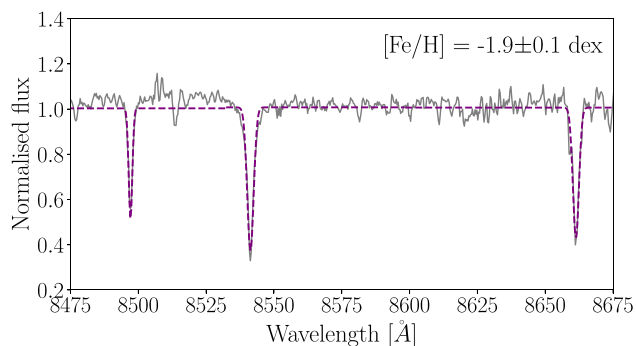$$+0.00155\,\Sigma Ca\,M \qquad (10)$$

Figure 4. The S/N weighted co-added spectra for the Ca(II) triplet region in And XXV. The purple dashed line is the fit to the Ca(II) triplet feature, the final derived metallicity is [Fe/H] = -1.9 ± 0.1 dex.
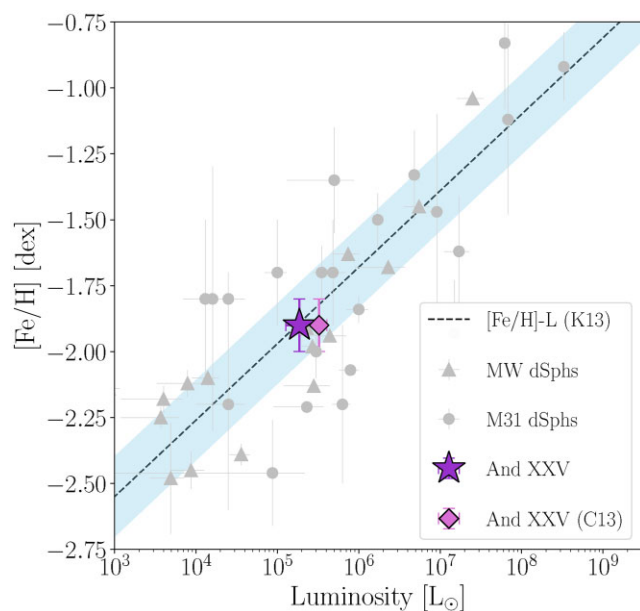

Figure 5. The luminosity–metallicity relation for LG dSphs. MW dSphs are represented by light grey triangles, whereas the M31 dSphs are the light grey circles. The pink diamond shows the results for And XXV from the C13 study and the purple star shows the result for And XXV from this study derived from the coadd spectra. The black dash line is the best fit luminosity–metallicity relation from Kirby et al. (2013) with the light blue band illustrating the 1σ scatter. And XXV is in perfect agreement with this relation.

where $\Sigma\text{Ca} = 0.5\text{EW}_{8498} + \text{EW}_{8542} + 0.6\text{EW}_{8662}$ and M is the absolute magnitude of each star given by:

$$M = V - 5 \times \log_{10}(D_\odot) + 5 \qquad (11)$$

where V is the S/N-weighted mean V-band magnitude of the 32 stars and $D_\odot$ is the heliocentric distance of the star which, for all stars, was assumed to be the heliocentric distance of And XXV, 751.6 kpc (Savino et al. 2022). This resulted in a metallicity for And XXV of [Fe/H] = -1.9 ± 0.1 dex. This value is in direct agreement with the result from the C13 study. Furthermore, this result is in agreement with the luminosity–metallicity relation (Kirby et al. 2013) for LG dwarfs, as shown in Fig. 5 with data taken from the sources mentioned for Fig. 3 in addition to Ho et al. (2015) and Wojno et al. (2020). We also obtained metallicities for individual stars. To do this we performed the same fitting procedure described above but

this time for each of the 32 spectra separately. From the individual metallicities, we produced a metallicity distribution function (MDF) from which we determined the mean metallicity of And XXV MCMC with an EMCEE routine fitting a Gaussian to the MDF. This analysis produced a metallicity in agreement with the result derived from the co-added spectra, albeit with a slightly larger uncertainty due to the larger systematic errors associated with the individual spectra with low S/N.

6 MASS MODELLING OF ANDROMEDA XXV

6.1 BINULATOR + GravSphere – mass modeling tool

GravSphere [1] is the dynamical mass modelling tool we used to measure the dark matter density profile of And XXV and is described described in detail in Read & Steger (2017); Read et al. (2018); Read et al. (2021); Genina et al. (2020b); Collins et al. (2021). In this section, we briefly review the GravSphere methodology and describe its application to And XXV. GravSphere solves the projected spherical Jeans equations (Jeans 1922; Binney & Mamon 1982) for a set of tracers, in this instance the 53 member stars of And XXV, to determine the dark matter density profile, assuming that it is a spherical, non-rotating system. These equations are known to have a mass-velocity anisotropy degeneracy for which a wide range of solution combinations can satisfy the model (Merrifield & Kent 1990; Wilkinson et al. 2002; Łokas & Mamon 2003; de Lorenzi et al. 2009). Several methods have been proposed to break this degeneracy (see e.g. Read & Steger (2017). GravSphere addresses it by fitting two higher order 'Virial Shape Parameters' (VSPs), first proposed by Merrifield & Kent [1990, see also Richardson & Fairbairn (2014)]. The velocity anisotropy profile is difficult to constrain observationally. However, using VSPs we only need line of sight velocities (easily obtained from spectroscopic observations) to place meaningful constraints on the velocity anisotropy profile, hence breaking the mass-velocity anisotropy degeneracy. GravSphere uses a symmetric version of the velocity anisotropy profile, $\tilde{\beta}$, is used to avoid issues with infinite values (Read et al. 2006), where $\tilde{\beta} = 0$ describes an isotropic velocity distribution, $\tilde{\beta} = -1$ a complete tangential and $\tilde{\beta} = 1$ a complete radial distribution. Finally, in line with previous studies (Read et al. 2018; Collins et al. 2021), we adopt the CORENFWTIDES model to describe the dark matter distribution. This mass profile includes within its parametrization the cusped Navarro–Frenk–White profile (NFW; Navarro et al. (1996b)). The NFW profile gives a good fit to dark matter density profiles in pure dark matter simulations and is described by two parameters: a virial mass M_{200} and concentration parameter c_{200}. The CORENFWTIDES model adds four new parameters to this: n, r_c, r_t, and δ. The first two control how 'cored' or 'cusped' the dark matter profile is inside r_c, where $n = 1$ corresponds to a constant density flat core, $n = 0$ corresponds to an r^{-1} cusp, as in the NFW profile, and $n = -1$ corresponds to an even steeper r^{-2} cusp. The second two parameters model the effect of tidal forces from a larger host galaxy stripping some of the outer mass away, where r_t is the tidal radius beyond which the density falls off as $r^{-\delta}$.

---

[1]The updated GravSphere code along with the new BINULATOR binning method, described in this paper and Collins et al. (2021), is available to download from https://github.com/justinread/gravsphere. pyGravSphere, a free form mass version of the GravSphere code (Genina et al. 2020b), is available to download from https://github.com/AnnaGenina/pygravsphere.

GravSphere has been rigorously tested on a wide variety of mock data (Read & Steger 2017; Read et al. 2018; Read et al. 2021; Genina et al. 2020b; Collins et al. 2021) and stands up well when compared to other dynamical mass modeling tools (Read et al. 2021). However, for systems with a small number of stars, and/or where the velocity uncertainty is large, the binning method in the previous version of GravSphere can become slightly biased towards cusped profiles (Gregory et al. 2019; Zoutendijk et al. 2021; Collins et al. 2021). To resolve this issue GravSphere was updated to include a new separate binning routing, BINULATOR, first introduced and outlined in detail in Collins et al. (2021). This update reduces the aforementioned biases by fitting a generalised Gaussian probability distribution to each bin, providing a robust estimate of the mean, variance, kurtosis, and corresponding uncertainties for each bin, even for systems with an extremely small sample size, such as And XXV. These estimates are then used as inputs to GravSphere. Detailed tests of this updated version of BINULATOR + GravSphere can be found in Collins et al. (2021) Appendix. A.

6.2 Implementing BINULATOR + GravSphere for Andromeda XXV

The surface brightness profile for And XXV was constructed from photometric data obtained through the LBT imaging described in Section 2.2. We included point sources from the entire data set out to $\sim 5 \times r_h$. For each star the radial distance from the centre of And XXV was measured and a probability of membership was assigned using the P_{dist} and method outlined in equation (1), albeit with a looser probability constraint ($P_{\text{member}} > 0.01$) and larger η parameters to ensure a representative and complete surface brightness profile. The velocity dispersion profile was constructed from the spectroscopic data for the 49 identified members of And XXV, using the velocity, velocity uncertainty, radial distance from the centre and the probability of membership determined using equation (7) for each member star. For both data sets the probability of membership is summed to give the total number of 'effective' tracers:

$$N_{\text{eff}} = \sum_{i=0}^{N_{\text{mem}}} P_{\text{mem,i}} \tag{12}$$

giving $N_{\text{eff}} = 2450$ for the photometric data and $N_{\text{eff}} = 27$ for the velocity data, which were then split into 98 bins of 25 and 3 bins of 9, respectively. GravSphere fits the surface brightness profile and radial velocity profile from the kinematic and photometric data input using an emcee routine (see Appendix A). For the parameters in the CORENFWTIDES profile we implemented the following priors: $7.5 < \log_{10}(M_{200}/\text{M}_{\odot}) < 11.5$, $7 < c_{200} < 53$, $-2 < \log_{10}(r_c/\text{kpc}) < 10$, $1 < \log_{10}(r_t/\text{kpc}) < 20$, $3 < \delta < 5$ and $-1 < n < 1$. For the symmetric velocity anisotropy, $\tilde{\beta}$, the priors were: $-0.1 < \tilde{\beta}_{\infty} < 1$, $-2 < \log_{10}(r_0/\text{kpc}) < 0$ and $1 < q < 3$. Finally, for the stellar mass of And XXV we convert the updated luminosity value from Savino et al. (2022) using the assumption of a stellar mass-to-light ratio of 2 for an old stellar population, in line with Simon (2019). This gives a stellar mass of $M_* = 7.5^{+0.6}_{-0.8} \times 10^5 \text{ M}_{\odot}$.

6.3 Dark matter density profile of Andromeda XXV

The resulting dark matter density profile is shown in Fig. 6. The dark grey and light grey shaded regions are the 1 and 2 σ uncertainties, respectively, and the purple dashed line is the half-light radius of And XXV. Within the uncertainties, it is not possible to distinguish between a cusped or cored profile. Instead, we turn our attention
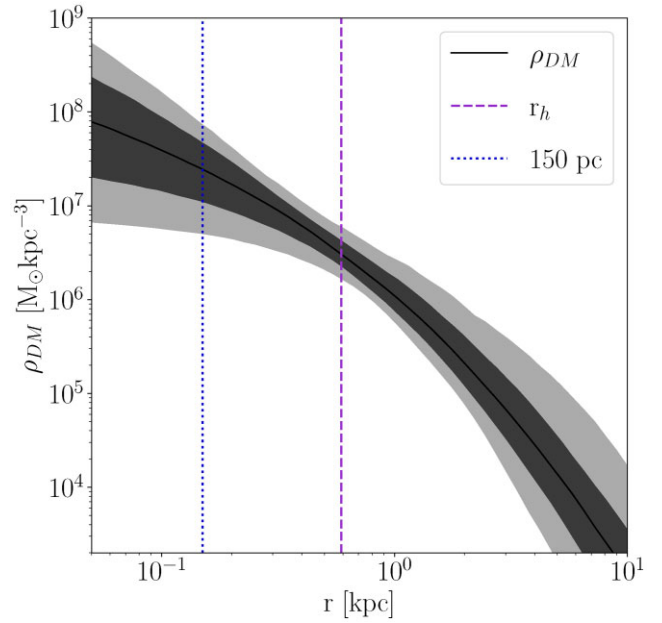

Figure 6. The dark matter density profile for And XXV. The dark grey and light grey shaded regions are the $1\times$ and $2\times$ σ uncertainties, respectively, and the purple dashed line is the literature half-light radius of And XXV (Savino et al. 2022). The blue dotted line corresponds to 150 pc, the radial distance at which we determine the central dark matter density (Read et al. 2018). And XXV has a low central dark matter density of $\rho_{\text{DM}}(150 \text{ pc}) = 2.3^{+1.4}_{-1.1} \times 10^7 \text{ M}_{\odot} \text{ kpc}^{-3}$.

to the central dark matter density, $\rho_{\text{DM}}(150\text{pc})$, illustrated by the blue dotted line. This value is used because this is the key region where core formation is expected to reduce dark matter densities, compared to CDM predictions (Read et al. 2018; Genina et al. 2020a). For And XXV, we get a central dark matter density of $\rho_{\text{DM}}(150 \text{ pc}) = 2.3^{+1.4}_{-1.1} \times 10^7 \text{ M}_{\odot} \text{ kpc}^{-3}$. This is low when compared to other LG dSphs, as shown in Fig. 7, with data taken from Read et al. (2019). Here dSphs are illustrated as circular data points and dIrrs are triangles. Quiescent (non-star forming) dwarfs are purple whereas currently star-forming dwarfs are blue. The pre-infall halo masses, M_{200} for the dwarfs in this study and the Read et al. (2019) sample are determined using an abundance matching method described in Read & Erkal (2019), which uses the the mean star formation rate averaged over the time when a galaxy was forming stars <SFR>, rather than stellar mass. This method was chosen as it is less susceptible to scatter associated with quenching or tidal interactions which can alter the M_{200} value obtained from traditional stellar mass abundance matching methods. This is particularly pertinent as And XXV may show signs of tidal stripping. The sample of dSph galaxies in Read et al. (2019) was chosen to be tidally isolated in order to measure the impact of dark matter heating on $\rho_{\text{DM}}(150 \text{ pc})$, independently of tidal effects. However, while the dSphs in Read et al. (2019) are known to be tidally isolated today (based on their orbits, measured using proper motion data from *Gaia* + HST (Gaia Collaboration et al. 2016, 2018), this does not mean that they have been tidally isolated for their whole history. As shown in Genina et al. (2020b), some dwarfs can have past interactions with one another and/or other infalling structure that lowers their inner densities while leaving them on apparently benign orbits today. While it is not possible to control for this for the dSphs in the Read et al. (2019) sample, like Fornax, such effects cannot explain the similarly low density of the isolated dIrrs in the Read et al. (2019) sample. Fornax
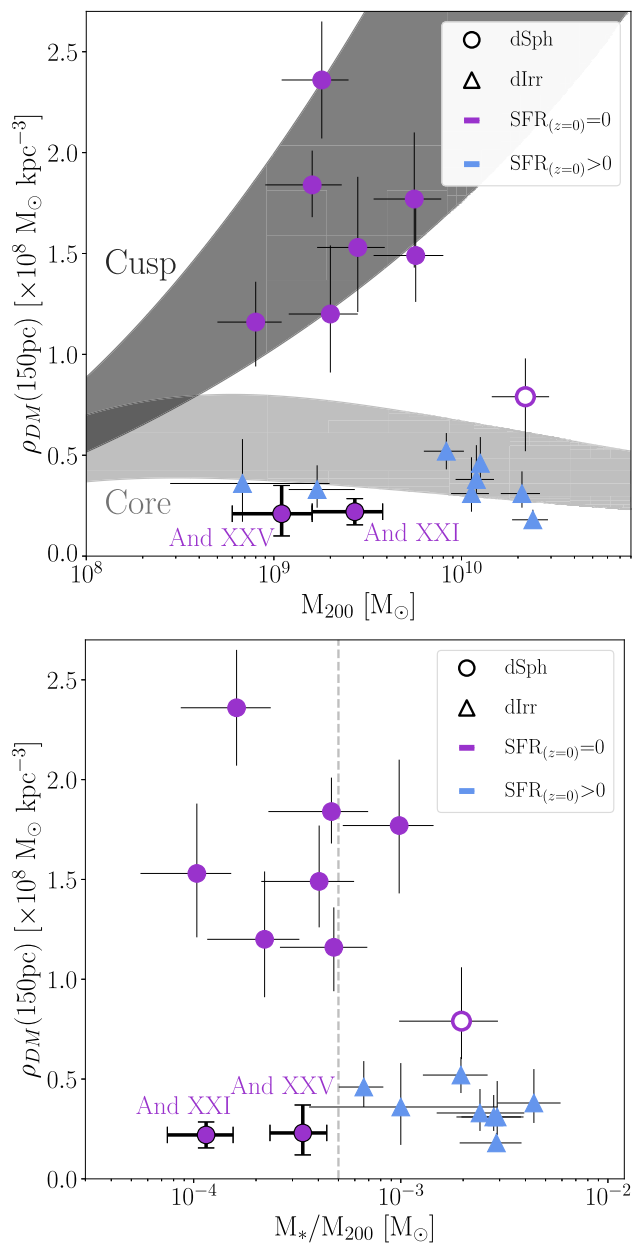
Figure 7. Top: The central dark matter density as a function of pre-infall mass, M_{200}. The dark grey band corresponds to the inner DM densities of completely cuspy profiles, whereas the light grey band corresponds to a fully cored coreNFW profile (Read et al. 2016). The width of the bands corresponds to the 1σ scatter in DM halo concentrations (Dutton & Macciò 2014). Bottom: Central dark matter density as a function of the stellar mass to halo mass ratio, M_*/M_{200}. The vertical grey dashed line illustrates the M_*/M_{200} ratio above which cusp-core transformations should become efficient (Di Cintio et al. 2014). Both: Circular data points are dSphs, whereas triangles are dIrrs. Dwarfs that are currently star forming are light blue whereas dwarfs that are quiescent are purple. Fornax is illustrated by the partially filled purple circular data point due to its unusual star formation history atypical of dSphs. The error bars are the 1σ uncertainties. And XXV and And XXI are labelled and have thicker error bars with caps. Data for And XXI were obtained from Collins et al. (2021) and from Read et al. (2019) for the other dwarfs.

is illustrated by the partially filled purple circular data point. Fornax is an interesting case that has a density and star formation history similar to dIrrs, but is a dSph. As such, its low density could owe to star formation (SF) and/or tides (Genina et al. 2022). A SF-induced

dark matter core provides the best fit to the kinematic data for Fornax, but tides could still have had a major influence even though Fornax's orbit looks to be tidally benign today.

When comparing And XXV to the rest of the LG dwarfs we can see just how low And XXV's central dark matter density is, at approximately an order of magnitude smaller than expected for a quiescent dSph, $\rho_{DM}(150\text{pc}) > 10^8 \, M_\odot \, \text{kpc}^{-3}$. Instead, And XXV has a central dark matter density more in line with currently star forming dIrrs, $\rho_{DM}(150\text{pc}) < 10^8 \, M_\odot \, \text{kpc}^{-3}$, which are expected to have lower central dark matter densities due to the dark matter heating effects of their continued star formation. Even when compared to the unusual Fornax, with even lower central density, And XXV is still a significant outlier. Furthermore, in the top panel in Fig. 7, the dark grey band corresponds to a fully cusped profile whereas the light grey band corresponds to a fully cored profile. The width of the bands corresponds to the 1σ scatter in DM halo concentrations (Dutton & Macciò 2014). Here we can see that And XXV appears to reside in the light grey region which corresponds to a fully cored profile. This behaviour is also reflected in And XXI, another documented M31 outlier for which we have dynamical mass modelling (Collins et al. 2021), as labelled in Fig. 7

7 DISCUSSION

Dark matter heating is one way in which dwarfs can lower the central dark matter densities. Could the unusually low central density observed in And XXV be due to dark matter heating caused by extended SF? From the shallow horizontal branch SF history, we can see that And XXV formed 50 per cent of its total stars 8.7 Gyrs ago and formed 90 per cent of stars (and thus likely finished star forming) 5.8 Gyrs ago (Weisz et al. 2019). It is possible that And XXV had a very short burst of SF ~1–2 Gyrs ago, although within the uncertainties this is not significant and could be an artefact of the method used as many of the dwarfs in their sample display this short burst. Deeper SF data are required to confirm the nature of this burst. Dark matter heating is more effective in galaxies with extended star formation (Read et al. 2016; Read et al. 2019); hence, the relatively short, isolated bursts of SF history that And XXV undergoes means it is unlikely that SF alone could explain the extremely low central density observed in And XXV. The same conclusion was reached for the other outliers with low central densities (Torrealba et al. 2019; Collins et al. 2021). However, in the bottom panel of Fig. 7 we can see that And XXV lies below the dashed grey line which indicates the stellar mass-halo mass ratio for which dark matter heating can become viable (Di Cintio et al. 2014). A recent study by Orkney et al. (2021) showed that gravitational fluctuations due to late minor mergers can also instigate slight core formation, even in dwarfs below this stellar mass-halo mass ratio. Therefore, it is possible that And XXV may have undergone a slight cusp-core transformation, although none of the simulated, isolated, dwarfs reported in Orkney et al. (2021) reach the low density of And XXV.

Another process that can lower the central density is tidal interactions. Tidal interactions lower densities at all radii, unlike dark matter heating which only lowers the central density. Tidal interactions can be split into two different processes, tidal stripping and tidal shocking. Tidal stripping occurs when the gravitational force from the host galaxy (in this case M31) exceeds the gravitational force from the dwarf allowing matter (dark matter/stars) to become unbound from the dwarf. Tidal stripping preferentially removes matter from the outer radii working inwards. As such the central dark matter density is only noticeably reduced after significant mass loss. For cusped profiles $\gtrsim 99$ per cent of the original mass would need to be lost

before the central dark matter density would decrease (Peñarrubia, Navarro & McConnachie 2008; Peñarrubia et al. 2010; Errani, Peñarrubia & Walker 2018; Errani & Peñarrubia 2020; Errani & Navarro 2021). However, cored profiles are less efficient at protecting their central densities and require less extreme mass loss for a noticeable effect (Read et al. 2006; Peñarrubia et al. 2010; Brooks & Zolotov 2014). Tidal shocking is another type of tidal interaction. It occurs for satellites on highly eccentric orbits moving in and out of the gravitational potential of the host. If the resulting gravitational fluctuations occur on shorter time scales than the dynamical time of the interaction, it will dynamically heat the stars and dark matter. The effect of tidal shocking is most pronounced at the pericentre of the orbit, as this is where the gravitational field changes most rapidly. Furthermore, tidal shocking is only effective at lowering central densities for cored systems (Read et al. 2006; Errani et al. 2017; Errani et al. 2018; Errani & Peñarrubia 2020; van den Bosch & Ogiya 2018) or for systems that reside in a low concentration dark matter halo (Amorisco 2019).

At a three-dimensional-projected distance of 85.2 kpc (Savino et al. 2022), And XXV is one of the closest M31 satellites, meaning it may potentially have had a previous encounter with M31 resulting in tidal forces. However, without proper motions, it is difficult to place meaningful constraints on the orbital history to ascertain if And XXV has had any close approaches with M31. Even armed with hypothetical proper motions, it is important to remember that the current orbital properties are not always a robust indicator of possible past close interactions (Lux, Read & Lake 2010; Genina et al. 2020a). Without orbital history information, we turn our attention to other potential indicators of tidal interaction. Firstly, we turn to the photometry to see if we can find indications of tidal interactions. No obvious tidal tails or other tidal substructure can be seen in the photometry of And XXV. The photometry used is shallow, as such tidal features, which tend to have low surface brightnesses, could readily be missed. Without dedicated deep imaging out to the very outskirts of And XXV, such tidal substructure would be difficult to detect (e.g. Shipp et al. 2022). Recent studies have shown that dSphs can undergo tidal interactions and show no observable tidal substructure (Read et al. 2006; Peñarrubia et al. 2009; Genina et al. 2020a), this is especially true for dwarfs on highly eccentric orbits, since the episodes of shocking are restricted to only the pericentric passages. As such, the dwarfs can relax back to equilibrium on a dynamical timescale, quickly erasing any signs of the interaction from the main body of the dwarf. Moreover, as the stellar component is strongly embedded in the dark matter halo, dSphs can be excessively stripped by tidal forces preferentially removing dark matter and as such, not demonstrate any observable tidal features in the stars until very extreme mass loss ($\gtrsim$ 90 per cent Peñarrubia et al. 2008; Peñarrubia et al. 2010; Errani et al. 2018). Secondly, in the kinematic analysis, we observed a kinematically colder centre in And XXV with the velocity dispersion increasing with radial distance. This may demonstrate that And XXV is not in dynamical equilibrium which could be due to previous tidal interactions, although it is important to note that within the uncertainties this flaring is not statistically significant. Interestingly a similar kinematic profile is observed in Antlia 2, a system for which tides are the suspected culprit (Torrealba et al. 2019). Moreover, the unusually low mass contained within the half-light radius measured for And XXV could be explained by tidal stripping/shocking, which would reduce the mass of the system over time. This is especially true for cored systems which are able to maintain their original radius while losing mass (Peñarrubia et al. 2010), resulting in the extended radial behaviour observed. Finally, dwarfs undergoing strong tidal interactions, which result in stellar

mass loss, are expected to be outliers on the luminosity–metallicity relation (e.g. Tucana III, see Simon et al. 2017). From Fig. 5 we can see that And XXV agrees with this relation which suggests it has not lost significant stellar mass through tides; an order of magnitude loss appears unlikely, but stripping ∼50 per cent of the stars may be allowed by the data. Furthermore, significant dark matter mass loss can lower the inner density, as can tidal shocking, without any associated stellar mass loss (e.g. Read et al. 2006).

No one piece of evidence is enough to decisively confirm or omit the possibility of either dark matter heating or tidal interactions as the cause of the low central density. However, the above would imply that we may potentially explain And XXV's extremely low central density due to a combination of both factors. Meaning And XXV could have undergone a slight cusp-core transformation from dark matter heating, which made And XXV more susceptible to tidal stripping and shocking which further reduced the central dark matter density, with tidal interactions being the significant contributing factor. This conclusion is in line with the results from studies investigating the other anomalous dwarfs (Torrealba et al. 2019; Collins et al. 2021). Although, detailed analysis in combination with additional data, such as proper motions, is required to consolidate this conclusion. And XXV joins the small but growing list of unusual LG 'puffy' dwarfs with low central densities. Around M31 we now see three such systems (And XXV, And XIX, and And XXI). A detailed study (Charles et al, in prep) into potential formation and evolution pathways resulting in the low central densities observed will improve our understanding of the nature of dark matter and potentially place constraints on different cosmological models.

8 CONCLUSIONS

We present an updated kinematic analysis for And XXV. And XXV was previously identified as a local group outlier. Using previous spectroscopic observations in combination with a new data set, providing 49 member stars, nearly double that in the previous study, we were sufficiently able to determine the presence of dark matter within And XXV, for the first time. In addition, we dynamically mass model And XXV using `BINULATOR` + `GravSphere` to constrain its dark matter density profile. Our key findings are as follows:

(i) We measure the a systemic velocity for And XXV of $v = -107.7 \pm 1.0 \text{ km s}^{-1}$ and a velocity dispersion of $\sigma_v = 3.7^{+1.2}_{-1.1} \text{ km s}^{-1}$ These values are consistent with the results derived by C13, which had a much smaller sample size.

(ii) We observe that the most central stars have a low velocity dispersion, which increases with increasing radial distance, potentially indicating And XXV is not in dynamical equilibrium and may have undergone tidal interactions.

(iii) Assuming dynamical equilibrium, we determine the mass contained within the half-light radius to be $M(r < r_h) = 4.7^{+3.0}_{-2.9} \times 10^6 \text{ M}_\odot$, which is lower than we would expect for the size of And XXV. This mass value corresponds to a mass-to-light ratio of $[M/L]_{r_h} = 25^{+17}_{-16} \text{ M}_\odot/\text{L}_\odot$, which, for the first time, indicates And XXV is a dark matter dominated system. Although within the uncertainties And XXV does not require dark-matter to explain the mass-to-light ratio, in agreement with C13.

(iv) For stars with a $S/N > 2.5$ we measure the metallicity of And XXV to be $[\text{Fe/H}] = -1.9 \pm 0.1$ dex from the coadded spectra. This is perfect in agreement with C13 and with the luminosity–metallicity relation for low-mass LG dwarfs (Kirby et al. 2013).

(v) Using the dynamical mass modelling tool `BINULATOR` + `GravSphere` we measure a low central dark matter density

of $\rho_{\mathrm{DM}}(150\,\mathrm{pc}) = 2.3^{+1.4}_{-1.1} \times 10^7\ \mathrm{M}_\odot\ \mathrm{kpc}^{-3}$. From the dark matter density profile alone we cannot distinguish between a cusped or cored halo. However, when compared to other quiescent star forming dSphs we find the And XXV has a central dark matter density approximately one order of magnitude smaller than we would expect, more similar to the central dark matter density of isolated star forming dIrrs.

(vi) In a companion paper (Charles et al in prep.), we will consider whether dark matter heating, tides, or some combination of these can explain And XXV's low density in the context of LCDM. We will also explore its implications for alternative dark matter models.

ACKNOWLEDGEMENTS

DATA AVAILABILITY

The raw spectra obtained with DEIMOS are available via the Keck archive. Fully reducedone-dimensional spectra and photometry will be made available upon reasonable request to the lead author. Electronic tables with the reduced properties (coordinates, magnitudes, velocities, and probability of membership) for all stars and the identified member stars will be provided on the journal website. The updated `GravSphere` code, along with the new BINULATOR binning method, is available to download from https://github.com/justinread/gravsphere.

REFERENCES

Agnello A., Evans N. W., 2012, ApJ, 754, L39
Amorisco N. C., 2019, MNRAS, 489, L22
Amorisco N. C., Evans N. W., 2012, ApJ, 756, L2
Armandroff T. E., Da Costa G. S., 1991, AJ, 101, 1329
Aubourg É. et al., 2015, Phys. Rev. D, 92, 123516
Battaglia G., Helmi A., Tolstoy E., Irwin M., Hill V., Jablonka P., 2008, ApJ, 681, L13
Binney J., Mamon G. A., 1982, MNRAS, 200, 361
Bond J. R., Kofman L., Pogosyan D., 1996, Nature, 380, 603
Brooks A. M., Zolotov A., 2014, ApJ, 786, 87
Buckley M. R., Peter A. H. G., 2018, Phys. Rep., 761, 1
Bullock J. S., Boylan-Kolchin M., 2017, ARA&A, 55, 343
Burles S., Nollett K. M., Truran J. W., Turner M. S., 1999, Phys. Rev. Lett., 82, 4176
Caldwell N. et al., 2017, ApJ, 839, 20
Collins M. L. M. et al., 2013, ApJ, 768, 172
Collins M. L. M. et al., 2014, ApJ, 783, 7
Collins M. L. M., Tollerud E. J., Sand D. J., Bonaca A., Willman B., Strader J., 2017, MNRAS, 467, 573
Collins M. L. M., Tollerud E. J., Rich R. M., Ibata R. A., Martin N. F., Chapman S. C., Gilbert K. M., Preston J., 2020, MNRAS, 491, 3496
Collins M. L. M. et al., 2021, MNRAS, 505, 5686
Cooper M. C., Newman J. A., Davis M., Finkbeiner D. P., Gerke B. F., 2012, spec2d: DEEP2 DEIMOS Spectral Pipeline. preprint(ascl:1203.003)
Cyburt R. H., 2004, Phys. Rev. D, 70, 023505
de Blok W. J. G., 2010, Adv. Astron., 2010, 789293
de Blok W. J. G., McGaugh S. S., Bosma A., Rubin V. C., 2001a, ApJ, 552, L23
de Blok W. J. G., McGaugh S. S., Bosma A., Rubin V. C., 2001b, ApJ, 552, L23
de Lorenzi F. et al., 2009, MNRAS, 395, 76
Di Cintio A., Brook C. B., Macciò A. V., Stinson G. S., Knebe A., Dutton A. A., Wadsley J., 2014, MNRAS, 437, 415
Dotter A., Chaboyer B., Jevremović D., Kostov V., Baron E., Ferguson J. W., 2008, ApJS, 178, 89
Dubinski J., Carlberg R. G., 1991, ApJ, 378, 496
Dutton A. A., Macciò A. V., 2014, MNRAS, 441, 3359
Errani R., Navarro J. F., 2021, MNRAS, 505, 18
Errani R., Peñarrubia J., 2020, MNRAS, 491, 4591
Errani R., Peñarrubia J., Laporte C. F. P., Gómez F. A., 2017, MNRAS, 465, L59
Errani R., Peñarrubia J., Walker M. G., 2018, MNRAS, 481, 5073
Faber S. M. et al., 2003, in Iye M., Moorwood A. F. M., eds, Society of Photo-Optical Instrumentation Engineers (SPIE) Conference Series, Vol. 4841, Instrument Design and Performance for Optical/Infrared Ground-based Telescopes. p. 1657
Fields B. D., 2011, Ann. Rev. Nucl. Part. Sci., 61, 47
Flores R. A., Primack J. R., 1994, ApJ, 427, L1
Foreman-Mackey D., Hogg D. W., Lang D., Goodman J., 2013, PASP, 125, 306
Fu S. W., Simon J. D., Alarcón Jara A. G., 2019, ApJ, 883, 11
Gaia Collaboration et al., 2016, A&A, 595, A2
Gaia Collaboration et al., 2018, A&A, 616, A1
Gao L., Springel V., White S. D. M., 2005a, MNRAS, 363, L66
Gao L., White S. D. M., Jenkins A., Frenk C. S., Springel V., 2005b, MNRAS, 363, 379
Genina A. et al., 2018, MNRAS, 474, 1398
Genina A., Read J. I., Fattahi A., Frenk C. S., 2022, MNRAS, 510, 2186
Genina A. et al., 2020b, MNRAS, 498, 144
Genina A., Read J. I., Fattahi A., Frenk C. S., 2022, MNRAS, 510, 2186
Gilbert K. M. et al., 2006, ApJ, 652, 1188
Gnedin O. Y., Zhao H., 2002, MNRAS, 333, 299
Gregory A. L., Collins M. L. M., Read J. I., Irwin M. J., Ibata R. A., Martin N. F., McConnachie A. W., Weisz D. R., 2019, MNRAS, 485, 2010
Ho N. et al., 2012, ApJ, 758, 124
Ho N., Geha M., Tollerud E. J., Zinn R., Guhathakurta P., Vargas L. C., 2015, ApJ, 798, 77
Ibata R., Sollima A., Nipoti C., Bellazzini M., Chapman S. C., Dalessandro E., 2011, ApJ, 738, 186
Irwin M., Lewis J., 2001, New A Rev., 45, 105
Jeans J. H., 1922, MNRAS, 82, 122
Kirby E. N., Cohen J. G., Guhathakurta P., Cheng L., Bullock J. S., Gallazzi A., 2013, ApJ, 779, 102
Kirby E. N., Simon J. D., Cohen J. G., 2015, ApJ, 810, 56
Kirby E. N., Cohen J. G., Simon J. D., Guhathakurta P., Thygesen A. O., Duggan G. E., 2017, ApJ, 838, 83
Komatsu E. et al., 2009, ApJS, 180, 330
Łokas E. L., Mamon G. A., 2003, MNRAS, 343, 401

Lux H., Read J. I., Lake G., 2010, MNRAS, 406, 2312

Marchesini D., D'Onghia E., Chincarini G., Firmani C., Conconi P., Molinari E., Zacchei A., 2002, ApJ, 575, 801

Martin N. F., Jin S., 2010, ApJ, 721, 1333

Martin N. F., Ibata R. A., Chapman S. C., Irwin M., Lewis G. F., 2007, MNRAS, 380, 281

Martin N. F. et al., 2009, ApJ, 705, 758

Martin N. F. et al., 2013a, ApJ, 772, 15

Martin N. F. et al., 2013b, ApJ, 779, L10

Martin N. F. et al., 2014, ApJ, 793, L14

Martin N. F. et al., 2016, ApJ, 833, 167

Mashchenko S., Wadsley J., Couchman H. M. P., 2008, Science, 319, 174

Mateo M. L., 1998, ARA&A, 36, 435

McConnachie A. W. et al., 2008, ApJ, 688, 1009

Merrifield M. R., Kent S. M., 1990, AJ, 99, 1548

Moore B., 1994, Nature, 370, 629

Moore B., Ghigna S., Governato F., Lake G., Quinn T., Stadel J., Tozzi P., 1999, ApJ, 524, L19

Navarro J. F., Eke V. R., Frenk C. S., 1996a, MNRAS, 283, L72

Navarro J. F., Frenk C. S., White S. D. M., 1996b, ApJ, 462, 563

Navarro J. F., Frenk C. S., White S. D. M., 1997, ApJ, 490, 493

Navarro J. F. et al., 2010, MNRAS, 402, 21

Newman A. B., Treu T., Ellis R. S., Sand D. J., 2013, ApJ, 765, 25

Oñorbe J., Boylan-Kolchin M., Bullock J. S., Hopkins P. F., Kereš D., Faucher-Giguère C.-A., Quataert E., Murray N., 2015, MNRAS, 454, 2092

Orkney M. D. A. et al., 2021, MNRAS, 504, 3509

Peebles P. J. E., 1982, ApJ, 263, L1

Peñarrubia J., Navarro J. F., McConnachie A. W., 2008, ApJ, 673, 226

Peñarrubia J., Navarro J. F., McConnachie A. W., Martin N. F., 2009, ApJ, 698, 222

Peñarrubia J., Benson A. J., Walker M. G., Gilmore G., McConnachie A. W., Mayer L., 2010, MNRAS, 406, 1290

Planck Collaboration et al., 2016, A&A, 594, A13

Planck Collaboration et al., 2020, A&A, 641, A6

Pontzen A., Governato F., 2012, MNRAS, 421, 3464

Read J. I., Erkal D., 2019, MNRAS, 487, 5799

Read J. I., Gilmore G., 2005, MNRAS, 356, 107

Read J. I., Steger P., 2017, MNRAS, 471, 4541

Read J. I., Wilkinson M. I., Evans N. W., Gilmore G., Kleyna J. T., 2006, MNRAS, 367, 387

Read J. I., Agertz O., Collins M. L. M., 2016, MNRAS, 459, 2573

Read J. I., Iorio G., Agertz O., Fraternali F., 2017, MNRAS, 467, 2019

Read J. I., Walker M. G., Steger P., 2018, MNRAS, 481, 860

Read J. I., Walker M. G., Steger P., 2019, MNRAS, 484, 1401

Read J. I. et al., 2021, MNRAS, 501, 978

Richardson T., Fairbairn M., 2014, MNRAS, 441, 1584

Richardson J. C. et al., 2011, ApJ, 732, 76

Sales L. V., Wetzel A., Fattahi A., 2022, Nat. Astron., 6, 897

Savino A., et al. 2022, ApJ, 938, 101.

Schlafly E. F., Finkbeiner D. P., 2011, ApJ, 737, 103

Shipp N. et al., 2022, ApJ, preprint (arXiv:2208.02255)

Simon J. D., 2019, ARA&A, 57, 375

Simon J. D., Geha M., 2007, ApJ, 670, 313

Simon J. D., Bolatto A. D., Leroy A., Blitz L., Gates E. L., 2005, ApJ, 621, 757

Simon J. D. et al., 2011, ApJ, 733, 46

Simon J. D. et al., 2015, ApJ, 808, 95

Simon J. D. et al., 2017, ApJ, 838, 11

Smith M. S., Kawano L. H., Malaney R. A., 1993, ApJS, 85, 219

Springel V. et al., 2005, Nature, 435, 629

Springel V., Frenk C. S., White S. D. M., 2006, Nature, 440, 1137

Starkenburg E. et al., 2010, A&A, 513, A34

Steigman G., 2007, Ann. Rev. Nucl. Part. Sci., 57, 463

Tegmark M. et al., 2006, Phys. Rev. D, 74, 123507

Tollerud E. J. et al., 2012, ApJ, 752, 45

Tollet E. et al., 2016, MNRAS, 456, 3542

Tolstoy E., Hill V., Tosi M., 2009, ARA&A, 47, 371

Torrealba G., Koposov S. E., Belokurov V., Irwin M., 2016, MNRAS, 459, 2370

Torrealba G. et al., 2019, MNRAS, 488, 2743

van den Bosch F. C., Ogiya G., 2018, MNRAS, 475, 4066

Walker M. G., Peñarrubia J., 2011, ApJ, 742, 20

Walker T. P., Steigman G., Schramm D. N., Olive K. A., Kang H.-S., 1991, ApJ, 376, 51

Walker M. G., Mateo M., Olszewski E. W., Gnedin O. Y., Wang X., Sen B., Woodroofe M., 2007, ApJ, 667, L53

Walker M. G., Mateo M., Olszewski E. W., Peñarrubia J., Evans N. W., Gilmore G., 2009, ApJ, 704, 1274

Walker M. G., McGaugh S. S., Mateo M., Olszewski E. W., Kuzio de Naray R., 2010, ApJ, 717, L87

Weisz D. R. et al., 2019, ApJ, 885, L8

Wilkinson M. I., Kleyna J., Evans N. W., Gilmore G., 2002, MNRAS, 330, 778

Wojno J., Gilbert K. M., Kirby E. N., Escala I., Beaton R. L., Tollerud E. J., Majewski S. R., Guhathakurta P., 2020, ApJ, 895, 78

Zolotov A. et al., 2012, ApJ, 761, 71

Zoutendijk S. L., Brinchmann J., Bouché N. F., den Brok M., Krajnović D., Kuijken K., Maseda M. V., Schaye J., 2021, A&A, 651, A80

SUPPORTING INFORMATION

Supplementary data are available at *MNRAS* online.

full_kinematics.txt
member_kinematics.txt

Please note: Oxford University Press is not responsible for the content or functionality of any supporting materials supplied by the authors. Any queries (other than missing material) should be directed to the corresponding author for the article.

APPENDIX A: RADIAL PROFILES FROM GravSphere

Here, we include the radial profile fits from GravSphere, see Fig. A1. First, the top panel shows the well-defined surface brightness profile, Σ_*. The blue data points are the binned photometry from the LBT imaging data out to four effective half light radii. Second, in the bottom panel is the radial velocity dispersion, σ_{LOS}. The blue data points are the binned velocity dispersion data taken from our probability weighted member stars. For both panels, the black line shows the fit from GravSphere with the dark and light grey shaded regions showing the 1 and 2σ uncertainty intervals respectively. The vertical purple dashed line is the half-light radius of And XXV. We see that the observed surface brightness profile is well reproduced by GravSphere. We note that the same velocity dispersion increasing with increasing radius behaviour is observed in the binned kinematic data that is explained in Section 4.2 and Section 7. We reiterate that this behaviour may indicate that And XXV is not in dynamical equilibrium and could be indicative of And XXV having undergone tidal interactions. The velocity dispersion profile inferred by GravSphere within the 1σ uncertainties for all bins. However, from visual inspection it seems possible that GravSphere has artificially biased the velocity dispersion to higher values at small radii in an attempt to fit this flaring feature. Although, this potential bias would not affect the conclusion that And XXV has an unusually low central dark matter density. A lower velocity dispersion profile would result in a lower density. As such, the value from this study can be considered an upper bound of the density.
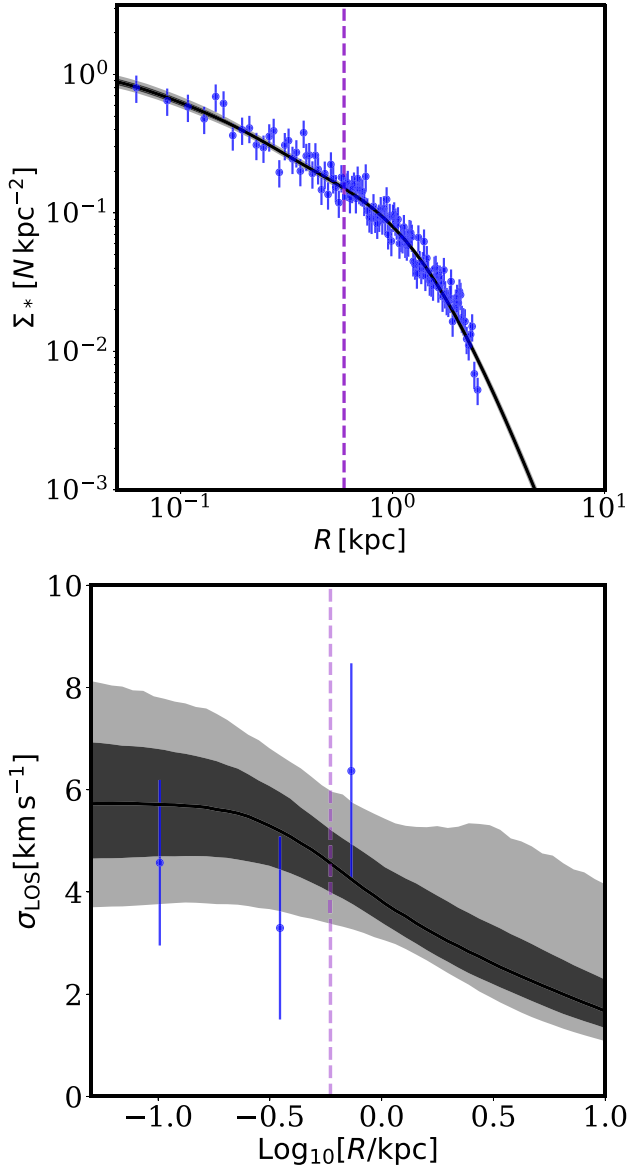
Figure A1. Top: The surface brightness profile, Σ_*. The blue data points are the binned photometry from the LBT imaging data. Bottom: The radial velocity dispersion, σ_{LOS}. The blue data points are the binned velocity dispersions from our probability weighted member stars. Both: The black line shows the fit from GravSphere. The 1 and 2σ uncertainty intervals are shown by the dark grey and light grey shaded regions, respectively. The vertical purple dashed line is the half-light radius of And XXV.

This paper has been typeset from a TEX/LATEX file prepared by the author.